Electric Feed System Pump Simulation for use in Bi-Propellant Rocket Propulsion Systems

Philip Wahl
philwahl@pdx.edu

Portland State University
ME448 - Computational Fluid Dynamics
March 22, 2019

1 Overview

Portland State Aerospace Society (PSAS) requires the development of an Electric Feed System (EFS) to satisfy the mass flow and pressure requirements of Launch Vehicle 4 (LV4). LV4 will utilize a bi-propellant propulsion system to generate the required thrust for the rocket to reach the Von Kármán Line, or the "Edge of Space", at approximately 100 km (or 62 mi) altitude. Liquid oxygen (LOX) and isopropyl alcohol (IPA) will be used as propellants. An EFS is an alternative to traditional pressure tanks or turbopumps used in larger and more expensive rockets. This paper details the computational fluid dynamic (CFD) simulation that has been performed to analyze the chamber pressure of the current EFS IPA pump design, which is shown in Figure 1. The findings from this analysis will be used to improve the design of the IPA pump. Additionally, they will serve as reference for modeling future LOX simulations.

The primary focus of this simulation is to understand the effects that impeller rotation in the pump case will have on the pressure and velocity distributions of the fluid. The fluid body of the pump will be modeled, starting from a mass flow inlet. The fluid enters this boundary and flows to the pump chamber housing the impeller, with an optimized rotation rate of approximately $36,000$ rpm. The impeller will be treated as a fluid wall rotating within the fluid body. The outlet on the diffuser side of the pump will be treated as a standard pressure outlet. The IPA pump will be modeled with the fluid at room temperature.

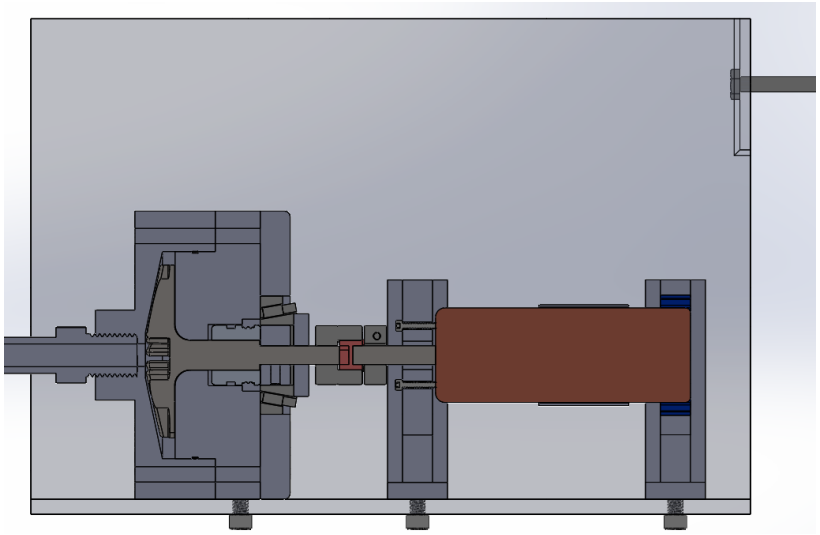

Figure 1: Cross-Section View of the Current Electric Feed System Design

1.1 Key Equations

Velocity from Mass Flow Rate[1]:

$$V = \frac{\dot{m}}{\rho A} \tag{1}$$

Reynold's Number[1]:

$$Re = \frac{\rho V D}{\mu} \tag{2}$$

Turbulence Intensity[2]:

$$I = 0.16 Re^{-1/8} \tag{3}$$

1.2 Nomenclature

- V: Inlet velocity
- $\dot{m}$: Mass flow rate
- ρ: Fluid density
- A: Inlet area
- D: Inlet diameter
- μ: Dynamic viscosity
- I: Turbulence intensity
- Re: Reynold's Number
- u_t: Impeller tip speed

2 Physical Model and Boundary Conditions:

The fluid continua for this simulation used a constant density, coupled flow model with $K - epsilon$ turbulence. Implicit integration and 2nd-order discretization were used. The inlet boundary was treated as a mass flow inlet with a fixed flow rate of $\dot{m} = 0.33\ kg/s$. Implicit unsteady flow physics was used, as steady flow resulted in residuals that would not converge.

The fluid body was treated as a stationary wall. The impeller wall was designated as a rotating reference frame within the fluid body, with a rotation motion of 35718 rpm rotating around the wall. A blended wall function with $E = 9.0$, $\kappa = 0.42$ was used. The impeller and fluid boundaries are shown in Figure 2b. The outlet boundary was set as a standard outlet. The flow pattern is visualized in Figure 2a. The inlet parameters are shown in Appendix A, Table 1.

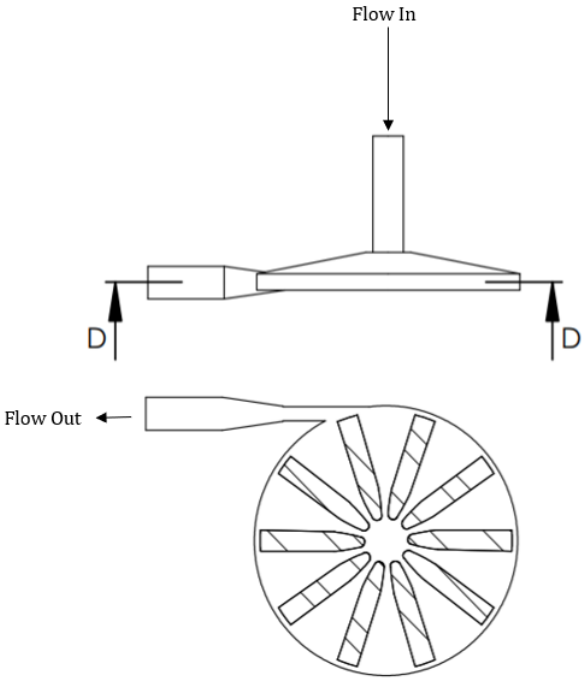

(a) Pump Flow Pattern Boundaries

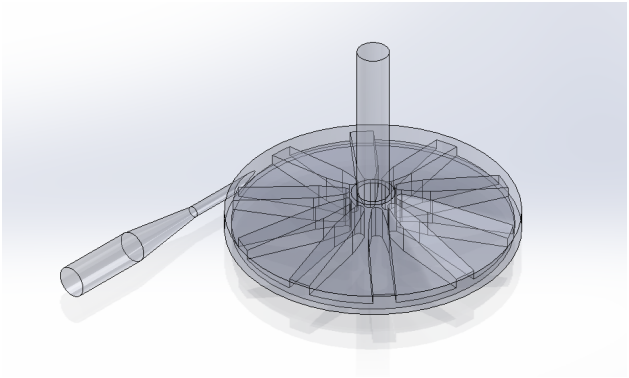

(b) Fluid Body With Impeller Walls Shown

Figure 2: Flow Boundaries

3 CFD Software Features

This simulation was considered a high turbulence case, with a turbulence intensity of $I = 0.046$ (found using Equation 3). This aligned with intuition, noting a high Reynold's number at $Re = 21711$. $K - Epsilon$ was selected as the turbulence model, as it provided the most optimal residuals within a reasonable number of iterations.

4 CFD Mesh

A polyhedral mesh was used with "Surface Remesher" enabled. The initial mesh used was 0.5 in, a course mesh relative to the size of the system being modeled. This mesh size converged for the first 80 iterations, but diverged sharply after this point, as shown in Figure 6. The mesh was then continually refined until an optimal base size of 0.2 in was determined. This base size resulted in acceptable convergence, with all residuals dropping below 0.001 while exhibiting reasonable computation times. The model converged in approximately 500 iterations. The course and fine mesh can be seen in Figure 3a and Figure 3b, respectively.

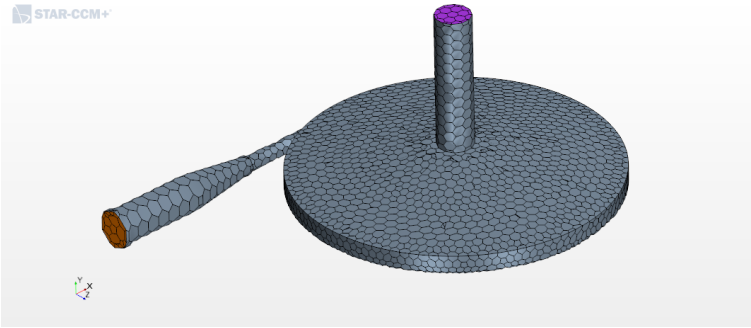

(a) Course Mesh (0.5 in)

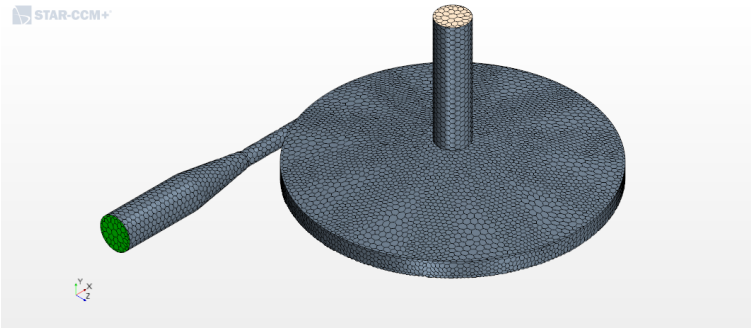

(b) Fine Mesh (0.2 in)

Figure 3: Mesh Scenes

5 Results and Discussion

The velocity vector scene of the pump at approximately 36000 rpm can be seen in Figure 5. The calculated impeller tip speed for the pump is 254 $\frac{m}{s}$. It can be seen that while the velocities at the impeller's edge are similar in magnitude to this target value, the precise velocity is not reached. This points to potential faults in the model's reference frame setup. Additionally, while rotational energy is being transferred to the pump chamber, it does not appear to be transferring proportionally to the flow outlet.

The pressure scalar cross-section shown in Figure 4 further illustrates this discrepancy. While the pump chamber in the model reaches the desired pressure range of 300-450 psi, the pressure leaving the pump at the diffuser is approximately 30% lower than inside the chamber. This could be caused either by the physics of the model, the boundary conditions selected, or the pump geometry itself. The residuals for this simulation can be seen in Figure 7.

Modeling the flow with a stagnation pressure inlet and pressure outlet provided the results shown Appendix A, Figure 9. While the pressure distribution in the chamber shows an appropriate gradient from the impeller eye out to the chamber wall, the pressure leaving the diffuser is also substantially lower than desired. Velocity inlet with mass flow out is also shown in Appendix B, Figure 8. This model resulted in appropriate pressure release into the diffuser, but gives an inlet pressure of approximately 225 psi, five times greater than the target inlet pressure of 45 psi.

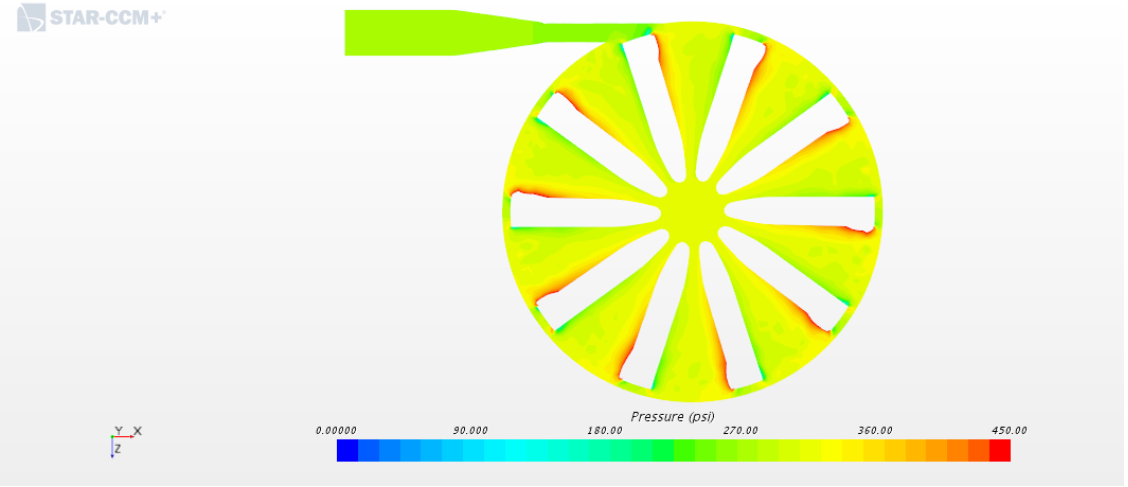

Figure 4: Pressure Distribution Cross-Section of Pump Chamber at ≈ 36000 rpm

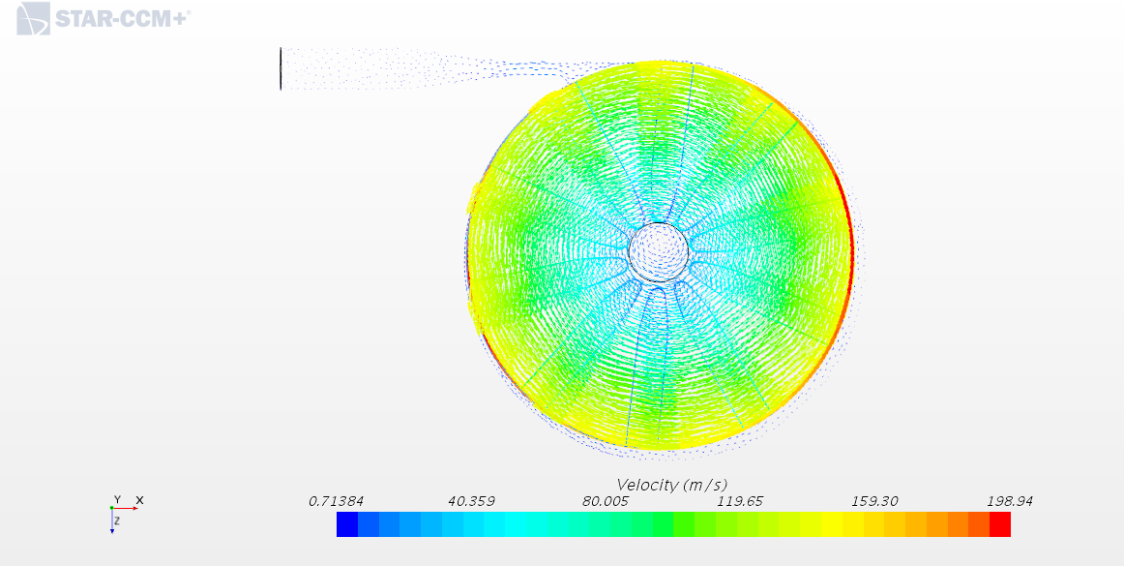

Figure 5: Velocity Profile of Pump Chamber at ≈ 36000 rpm

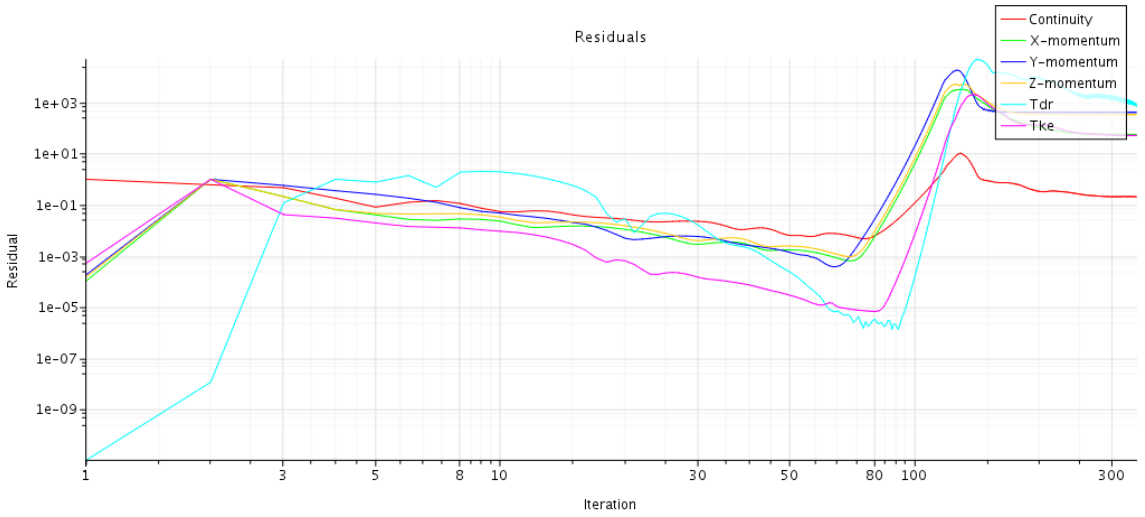

Figure 6: Divergent Residuals for Course Mesh (0.5 *in* Base Size)

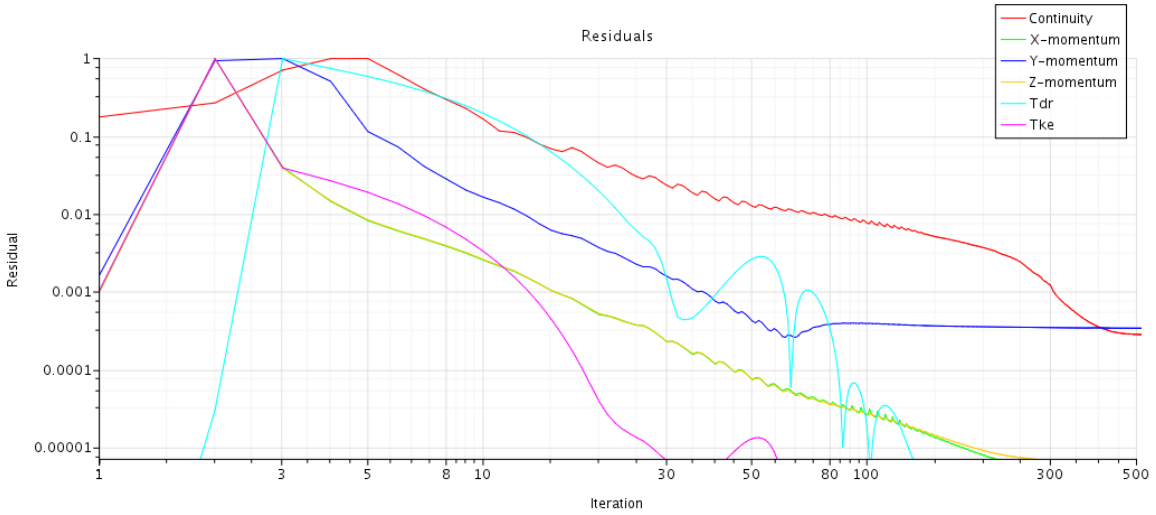

Figure 7: Converged Residuals for Fine Mesh (0.2 *in* Base Size)

6 Conclusion

While the results from this simulation have not provided an accurate model of the theoretical pump design, it points toward several areas of improvement, both for CFD modeling of the pump and the design itself. The primary area of concern with the simulation's results is the drop in pressure from the pump chamber to the outlet. Multiple boundary condition configurations were tested, including mass flow inlet with pressure outlet, stagnation inlet with mass flow outlet, stagnation inlet with pressure outlet, and velocity inlet with pressure outlet. The pressure distributions of alternative boundary condition configurations can be seen in Appendix B, Figure 8 and Figure 9. Moving forward, the boundary conditions of this model will continue to be reconfigured to achieve the optimal pressure results.

The fluid physics continua could also be a cause of the discrepancies in the results. A possible alternative is to reconstruct the model to simulate the rotation of the impeller as a solid rather than a fluid wall. It is possible the the transfer of energy in the simulation is not properly represented without the inertia of the solid body accounted for.

Finally, the results could point toward the need to improve the pump design itself. Moving forward, CFD models with alternative outlet diameters will continue to be tested to see if the pump's design can be optimized to further resist flow in the system. Additionally, the pump volute design can potentially be improved to optimize the flow pattern for greater pressure gain. Currently, the pump chamber is concentric about the impeller. However, traditional pump volutes feature a unique flow path that diverges at the outlet to convert kinetic energy from velocity to pressure[1]. This configuration will be modeled in the future to compare to the final results that are found for the concentric chamber.

Appendices

Appendix A: Tables

Table 1: Inlet Flow Properties of IPA[1]

Property	Symbol	Units	Value
Area	A	$[mm^2]$	81.07
Mass Flow	$\dot{m}$	$[\frac{lg}{s}]$	0.33
Velocity	V	$[\frac{m}{s}]$	5.17
Pressure	P	[psi]	45
Temperature	T	$[°C]$	20
Dynamic Viscocity	μ	$[Pa \cdot s]$	0.0019
Density	ρ	$[\frac{kg}{m^3}]$	786
Reynold's Number	Re	[-]	21711
Turbulence Intensity	I	[-]	0.046

Appendix B: Additional Figures

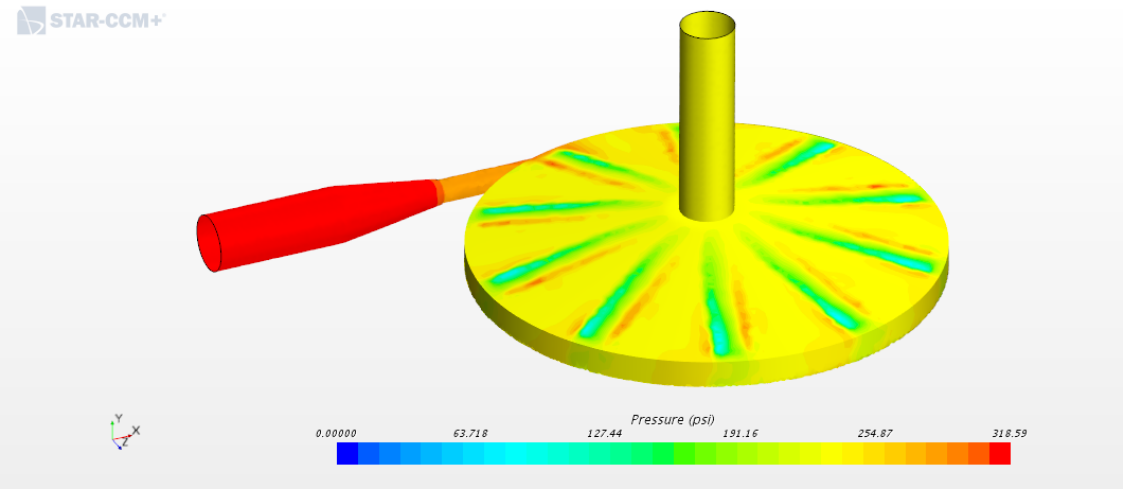

Figure 8: Pressure Distribution With Velocity In, Mass Flow Out BCs

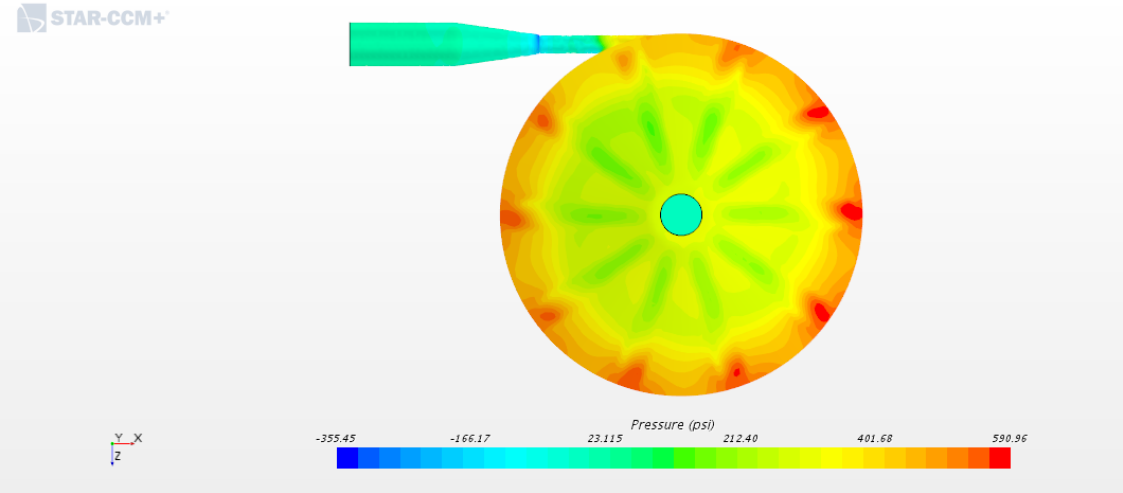

Figure 9: Pressure Distribution With Pressure In, Pressure Out BCs

Appendix C: References

[1] T. Bergman & F. Incropera (2011),"Fundamentals of Heat and Mass Transfer" ($7^{th}Ed$).

[2] ANSYS, Inc. (2018), "ANSYS Fluent User's Guide, Release 19.0", Equation (6.68).